LETTER

doi:10.1038/nature11306

# Neuronal circuitry mechanism regulating adult quiescent neural stem-cell fate decision

Juan Song[1,2], Chun Zhong[1,2], Michael A. Bonaguidi[1,2], Gerald J. Sun[1,3], Derek Hsu[1], Yan Gu[4], Konstantinos Meletis[5], Z. Josh Huang[6], Shaoyu Ge[4], Grigori Enikolopov[6], Karl Deisseroth[7], Bernhard Luscher[8], Kimberly M. Christian[1,2], Guo-li Ming[1,2,3] & Hongjun Song[1,2,3]

**Adult neurogenesis arises from neural stem cells within specialized niches[1–3]. Neuronal activity and experience, presumably acting on this local niche, regulate multiple stages of adult neurogenesis, from neural progenitor proliferation to new neuron maturation, synaptic integration and survival[1,3]. It is unknown whether local neuronal circuitry has a direct impact on adult neural stem cells. Here we show that, in the adult mouse hippocampus, nestin-expressing radial glia-like quiescent neural stem cells[4–9] (RGLs) respond tonically to the neurotransmitter γ-aminobutyric acid (GABA) by means of $\gamma_2$-subunit-containing $GABA_A$ receptors. Clonal analysis[9] of individual RGLs revealed a rapid exit from quiescence and enhanced symmetrical self-renewal after conditional deletion of $\gamma_2$. RGLs are in close proximity to terminals expressing 67-kDa glutamic acid decarboxylase (GAD67) of parvalbumin-expressing ($PV^+$) interneurons and respond tonically to GABA released from these neurons. Functionally, optogenetic control of the activity of dentate $PV^+$ interneurons, but not that of somatostatin-expressing or vasoactive intestinal polypeptide (VIP)-expressing interneurons, can dictate the RGL choice between quiescence and activation. Furthermore, $PV^+$ interneuron activation restores RGL quiescence after social isolation, an experience that induces RGL activation and symmetrical division[8]. Our study identifies a niche cell–signal–receptor trio and a local circuitry mechanism that control the activation and self-renewal mode of quiescent adult neural stem cells in response to neuronal activity and experience.**

Recent genetic lineage-tracing studies have identified nestin-expressing RGLs as quiescent neural stem cells (qNSCs) in the adult mouse hippocampus[4–9]. In adult *nestin–GFP* mice[10], cells expressing green fluorescent protein ($GFP^+$ cells) in the subgranular zone (SGZ) with radial processes expressed GFAP (glial fibrillary acidic protein) but rarely MCM2 (minichromosome maintenance type 2), indicating quiescence (Supplementary Fig. 1a, b). To assess whether local interneurons regulate adult qNSCs directly by means of neurotransmitter release, we examined RGL responses to GABA in slices acutely prepared from adult *nestin–GFP* mice by electrophysiology (see Methods). $GFP^+$ RGLs recorded under whole-cell voltage-clamp showed prominent responses to GABA (200 mM) or the $GABA_A$ receptor ($GABA_AR$) agonist muscimol (200 mM), which were abolished by the $GABA_AR$ antagonist bicuculline (BMI; 50 μM; Supplementary Fig. 1c, d). GABA responses were potentiated by diazepam (1 μM), which specifically enhances $\gamma_2$-containing $GABA_AR$ responses to GABA[11]. Indeed, $GFP^+$ RGLs showed immunoreactivity to $\gamma_2$ (Supplementary Fig. 1e). $\gamma_2$-containing $GABA_ARs$ are present in non-neuronal cells and can be found both outside and inside synapses in mature neurons[11]. No spontaneous or evoked synaptic currents in response to field stimulation of the dentate granule cell layer were detected in $GFP^+$ RGLs ($n = 25$ cells; Supplementary Fig. 1f, g). Instead, tonic GABA responses were recorded ($n = 18$ cells; Fig. 1 and Supplementary Fig. 1g, h), suggesting GABA spill-over from nearby synapses[11]. To exclude the possibility of synaptic inputs with low release probabilities, we applied hypertonic solution to enhance presynaptic release[12]. Increased GABA tonic responses, but not synaptic currents, were observed (Supplementary Fig. 1h). Inhibition of the GABA reuptake transporter GAT1 with NO-711 (10 μM) also increased tonic responses (Fig. 1), further supporting the tonic nature of GABAergic responses in RGLs.

We next explored pharmacological properties of tonic GABA responses in RGLs[13]. Consistent with the $\gamma_2$ involvement, diazepam (1 μM) significantly increased tonic responses, whereas the benzodiazepine antagonist flumazenil (10 μM) decreased them (Fig. 1). The $\alpha_5$-selective benzodiazepine agonist midazolam (10 μM), or the $\beta_3$-selective positive allosteric modulator etomidate (ETMD; 100 nM), increased tonic GABA responses, whereas the $\alpha_5$-selective inverse agonist L-655708 (50 μM) decreased this response (Fig. 1). Together, these results suggest that $\alpha_5\beta_3\gamma_2$ $GABA_ARs$ are present in adult dentate RGLs to mediate tonic responses to GABA.

To examine the functional role of GABA in regulating adult dentate RGLs *in vivo*, we assessed 5-ethynyl-2′-deoxyuridine (EdU) incorporation and MCM2 expression by RGLs after treatment with diazepam (Supplementary Fig. 2a). We identified RGLs as SGZ cells with $nestin^+$ radial processes (Fig. 2a). Stereological quantification showed that treatment with diazepam led to a 45% decrease in the number of $EdU^+$ RGLs compared with vehicle treatment (Fig. 2b). The number

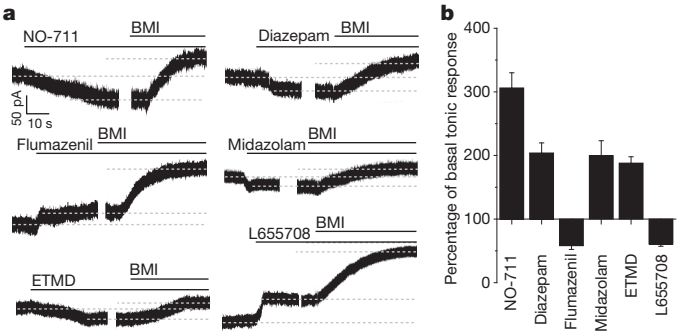


**Figure 1 | Tonic activation of adult quiescent neural stem cells by GABA by means of $\alpha_5\beta_3\gamma_2$ $GABA_ARs$.** **a**, Sample traces of whole-cell voltage-clamp recording from $GFP^+$ RGLs treated with diazepam (1 μM), flumazenil (10 μM), midazolam (10 μM), ETMD (100 nM) or L-655708 (50 μM), followed by BMI (100 μM) to obtain a baseline for normalizing tonic responses for each cell. **b**, Summary of normalized amplitude of tonic response. Values are means and s.e.m. ($n = 4$ or 5 cells; all significantly different from the basal condition; $P < 0.05$; Student's *t*-test).

[1]Institute for Cell Engineering, Johns Hopkins University School of Medicine, Baltimore, Maryland 21205, USA. [2]Department of Neurology, Johns Hopkins University School of Medicine, Baltimore, Maryland 21205, USA. [3]The Solomon H. Snyder Department of Neuroscience, Johns Hopkins University School of Medicine, Baltimore, Maryland 21205, USA. [4]Department of Neurobiology and Behaviour, State University of New York at Stony Brook, New York 11794, USA. [5]Department of Neuroscience, Karolinska Institutet, S-171 77 Stockholm, Sweden. [6]Cold Spring Harbor Laboratory, Cold Spring Harbor, New York 11724, USA. [7]Department of Bioengineering, Stanford University, Stanford, California 94305, USA. [8]Department of Biology, Pennsylvania State University, University Park, Pennsylvania 16802, USA.

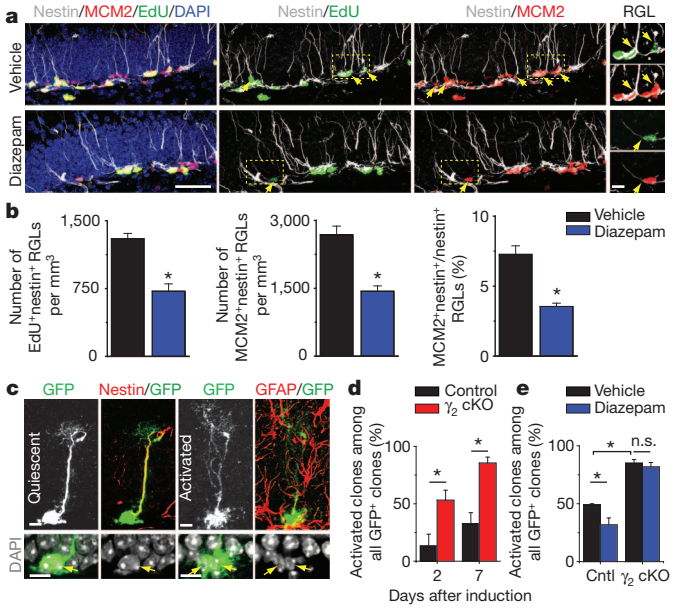


**Figure 2 | Cell-autonomous role of $\gamma_2$-containing $GABA_A$Rs in maintaining adult neural stem cell quiescence.** **a**, **b**, Diazepam promotes quiescence of nestin$^+$ RGLs in the adult dentate gyrus. **a**, Sample confocal images of immunostaining of nestin, MCM2, EdU and 4′,6-diamidino-2-phenylindole (DAPI). Arrows indicate nestin$^+$MCM2$^+$ or nestin$^+$EdU$^+$ RGLs. Scale bars, 50 μm (left) and 10 μm (last column). **b**, Summaries of stereological quantification of RGL EdU incorporation and MCM2 expression. Values are means and s.e.m. ($n = 4$ animals; asterisk, $P < 0.01$; Student's $t$-test). **c**–**e**, $\gamma_2$ deletion in individual RGLs leads to their activation. **c**, Sample confocal images of immunostaining. Scale bars, 10 μm. **d**, **e**, Summaries of percentages of RGL clones that were activated (**d**) and those treated with vehicle or diazepam at 7 days after induction (**e**) for control (cntl) and cKO mice. Values are means and s.e.m. ($n = 4$–8 animals; asterisk, $P < 0.01$; n.s., $P > 0.1$; Student's $t$-test).

of MCM2$^+$nestin$^+$ RGLs and the percentage of RGLs that were MCM2$^+$ were also significantly decreased (Fig. 2b). Thus, systemic enhancement of $\gamma_2$-mediated GABA signalling promotes adult dentate RGL quiescence at the population level.

To examine a cell-autonomous role of $\gamma_2$ in RGLs, we generated *nestin-CreER$^{T2+/-}$;Z/EG$^{f/-}$;$\gamma_2^{f/f}$* (cKO) mice and *nestin-CreER$^{T2+/-}$;Z/EG$^{f/-}$;$\gamma_2^{+/+}$* (control) mice and used a low dose of tamoxifen for sparse induction to perform clonal analysis of adult RGLs[9] (Supplementary Fig. 2b–d). Immunohistology and electrophysiology indicated highly efficient, but not complete, $\gamma_2$ deletion in GFP$^+$ RGLs (Supplementary Fig. 2e, f). In cKO mice, the percentage of RGL clones that were activated increased markedly compared with control mice at 2 and 7 days after induction (Fig. 2c, d). Treatment with diazepam decreased the percentage of activated RGL clones in control mice at 7 days after induction, but had no effect in cKO mice (Fig. 2e and Supplementary Fig. 2g). These results showed a direct role of GABA in maintaining adult NSC quiescence through $\gamma_2$ signalling.

We next examined the fate choice of activated RGLs. There was a marked increase in pairs of closely associated GFP$^+$ RGLs at 2 days after induction in adult cKO mice compared with controls, indicating increased RGL symmetrical self-renewal (Fig. 3a, b). Detailed analysis at 7 days after induction showed increased symmetrical and astrogliogenic asymmetrical RGL division in cKO mice (Fig. 3c). Conversely, treatment with diazepam decreased RGL symmetrical division and astrogliogenic asymmetric division in control mice, but had no effect in cKO mice (Fig. 3d). In supporting short-term lineage-tracing results, analysis of clonal composition at 30 days after induction showed decreased percentages of quiescent clones and an increased percentage of clones with multiple RGLs in cKO mice (Fig. 3e, f and Supplementary Fig. 3). Consistent with a role of GABA signalling in promoting new neuron survival[14], percentages of neurogenic clones

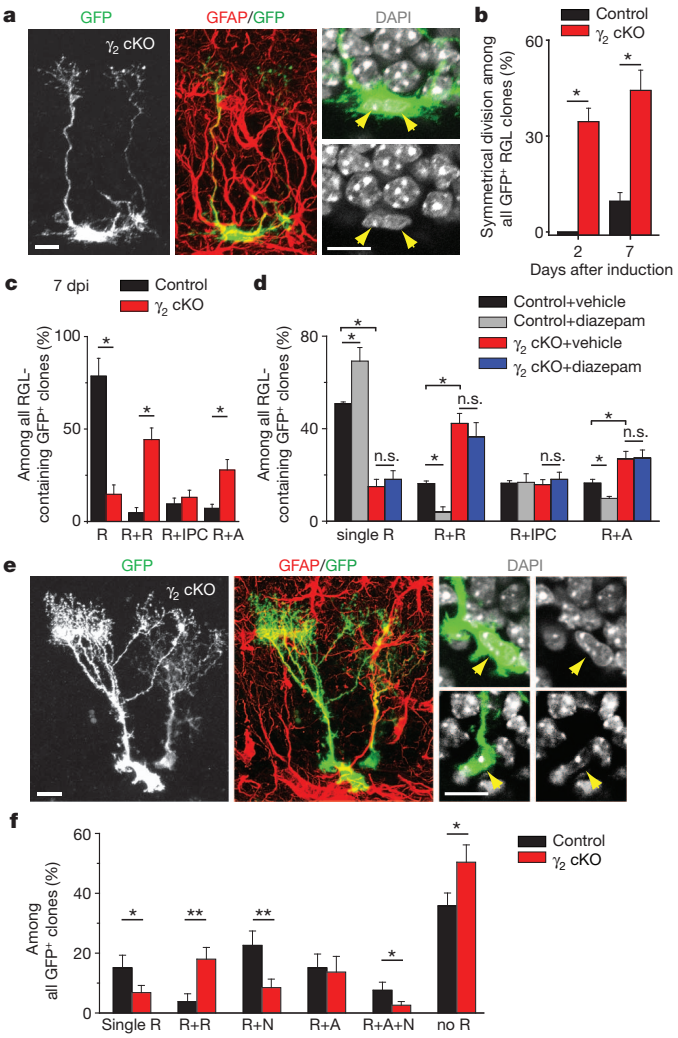


**Figure 3 | Clonal analysis of RGL fate choice after conditional $\gamma_2$ deletion in individual RGLs in the adult dentate gyrus.** **a**–**d**, Short-term effect of $\gamma_2$ deletion on the activation and fate choice of adult dentate RGLs. **a**, Sample confocal images of immunostaining for a GFP$^+$ clone indicating symmetrical division at 7 days after induction. Scale bars, 10 μm. **b**–**d**, Summaries of percentages of clones indicating symmetrical divisions at 2 and 7 days after induction (**b**), and percentages of different types of RGL clones (**c**) and those treated with vehicle or diazepam (**d**) at 7 days after induction: R + R (two RGLs), R + intermediate progenitor cell (IPC; one RGL and one GFAP$^-$ IPC) and R + A (one RGL and one GFAP$^+$ bushy astrocyte). Values are means and s.e.m. ($n = 4$–8 animals; asterisk, $P < 0.05$; n.s., $P > 0.1$; Student's $t$-test). **e**, **f**, Long-term effect (at 30 days after induction) of $\gamma_2$ deletion on the composition of GFP$^+$ clones in the adult dentate gyrus. **e**, Sample confocal images of immunostaining for a clone consisting of two GFAP$^+$ cells with radial processes. Scale bars, 10 μm. **f**, Summary of percentages of different clone types among all GFP$^+$ clones: R, RGL; N, IPC or neuron; A, astrocyte. Values are means and s.e.m. ($n = 4$–8 animals; asterisk, $P < 0.05$; two asterisks, $P < 0.01$; Student's $t$-test).

and multilineage clones were decreased significantly (Fig. 3f and Supplementary Fig. 3e). In contrast, clones without any RGLs were increased in cKO mice (Fig. 3f), suggesting increased RGL depletion after $\gamma_2$ deletion. Together, these gain-of-function and loss-of-function analyses identified GABA as a niche signal to maintain adult NSC quiescence and inhibit symmetrical self-renewal and astrocyte fate choice through $\gamma_2$-containing $GABA_A$Rs under basal physiological conditions.

We next sought to identify GABA-releasing niche cells among multiple interneuron subtypes in the adult dentate gyrus[15,16]. Immunohistological analysis of adult *nestin–GFP* mice showed a close association between GFP$^+$ RGLs and GAD67$^+$ terminals from PV$^+$

interneurons (Fig. 4a and Supplementary Movie 1). To determine whether $PV^+$ interneurons interact functionally with RGLs, we took an optogenetic approach and used double-floxed (DIO) adeno-associated virus (AAV) to express channelrhodopsin-2 (ChR2) or halorhodopsin (eNpHR3.0) specifically in $PV^+$ interneurons, using adult *PV-Cre* mice[17] (Supplementary Fig. 4a). Immunostaining and electrophysiology confirmed the specificity and efficacy of AAV-mediated opsin expression in controlling the firing of dentate $PV^+$ interneurons (Supplementary Fig. 4b–e). In acute slices from *PV-Cre*$^{+/-}$;*nestin–GFP*$^{+/-}$ mice, photoactivation of $PV^+$ interneurons induced synaptic responses in mature dentate granule cells and tonic responses in $GFP^+$ RGLs to GABA (Fig. 4b, c). Furthermore, a decrease in GABA turnover with the GABA transaminase inhibitor vigabatrin (100 μM) drastically increased $GFP^+$ RGL responses to $PV^+$ interneuron activation (Fig. 4c). Together, these results indicate that adult RGLs respond tonically to GABA released from local $PV^+$ interneurons.

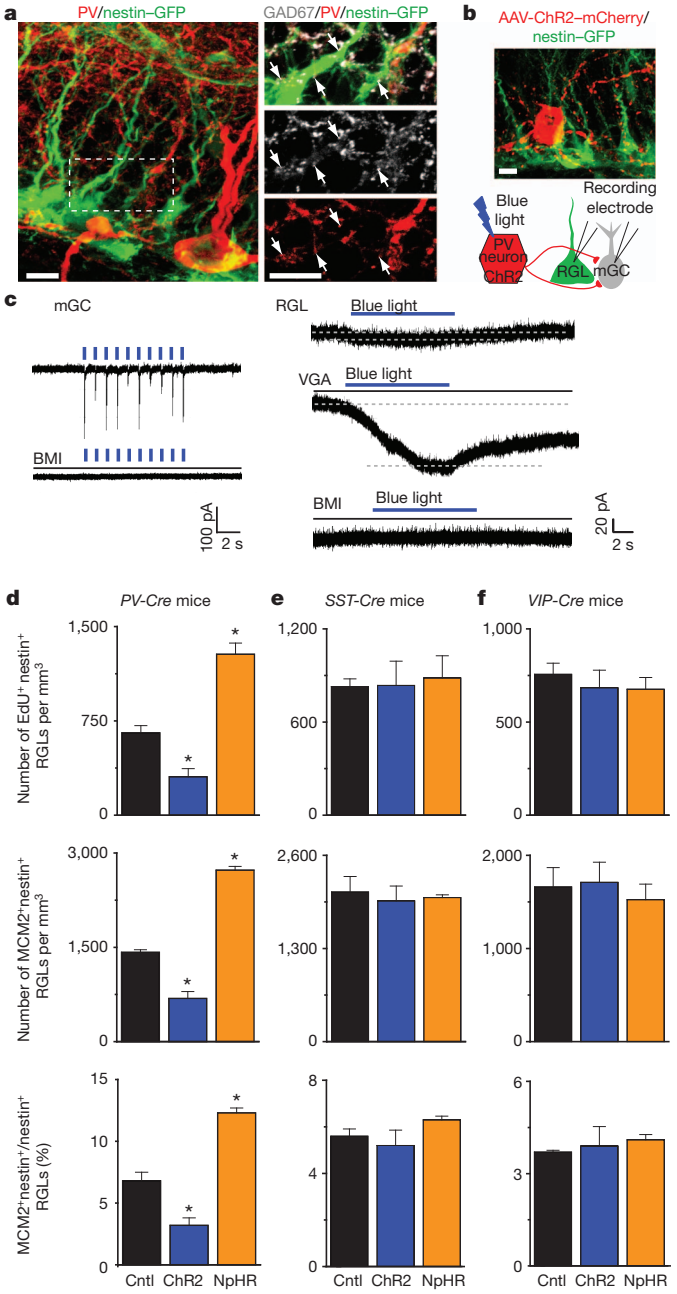


**Figure 4 | Regulation of quiescence and activation state of neural stem cells by $PV^+$, but not $SST^+$ or $VIP^+$ interneuron activity, in the adult dentate gyrus.** **a**, Sample confocal images of GFP and immunostaining of PV and GAD67 (See Supplementary Movie 1). Scale bars, 5 μm. **b**, Sample confocal image and schematic diagram of electrophysiological recording. Scale bar, 10 μm. **c**, Sample whole-cell voltage-clamp recording traces of responses after light stimulation of $ChR2^+PV^+$ interneurons from a mature granule cell (mGC; 1 Hz) and a $GFP^+$ RGL (8 Hz) in acute slices, and after treatment with BMI (50 μM) or vigabatrin (VGA; 100 μM). **d**–**f**, Regulation of RGL activation in the adult dentate gyrus by local interneuron activity. Shown are summaries of stereological quantification of RGL EdU incorporation and MCM2 expression after *in vivo* activation (ChR2) or suppression (NpHR) of $PV^+$ (**d**), $SST^+$ (**e**) or $VIP^+$ (**f**) interneurons or sham treatment (cntl; see Supplementary Figs 5a and 6e for experimental procedures). Values are means and s.e.m. ($n = 3$ or 4 animals; asterisk, $P < 0.01$; Student's *t*-test).

To assess the functional impact of $PV^+$ interneuron activity on RGL behaviour, we photoactivated or suppressed $PV^+$ interneurons in the dentate gyrus of adult *PV-Cre* mice for 5 days (Supplementary Fig. 5a). In comparison with sham treatment without light stimulation, EdU incorporation and MCM2 expression by RGLs were significantly decreased after activation of $PV^+$ interneurons expressing ChR2 tagged with yellow fluorescent protein (ChR2–YFP), resulting in a 53% decrease in RGL activation at the population level (Fig. 4d and Supplementary Fig. 5b). Conversely, suppression of $PV^+$ interneurons expressing eNpHR–YFP led to a 95% increase in RGL activation (Fig. 4d). These results identified $PV^+$ interneurons as a critical niche component and showed that $PV^+$ interneuron activity can dictate the RGL choice between quiescence and activation in the adult dentate gyrus.

Do other subtypes of local interneurons also regulate RGL behaviour *in vivo*? We developed similar optogenetic strategies to manipulate somatostatin-expressing ($SST^+$) or vasoactive intestinal polypeptide-expressing ($VIP^+$) interneurons[16] (Supplementary Fig. 6a). Both $SST^+$ and $VIP^+$ interneurons showed elaborated processes in the SGZ and hilus region (Supplementary Fig. 6c, d and Supplementary Movie 2), and our procedure labelled greater numbers of $SST^+$ and $VIP^+$ interneurons than $PV^+$ interneurons in the adult dentate gyrus (Supplementary Fig. 6b). Electrophysiological recoding of $GFP^+$ RGLs did not detect any tonic or synaptic responses after light-induced activation of $SST^+$ or $VIP^+$ interneurons in acute slices (Supplementary Fig. 6c, d). Functionally, photoactivated or suppressed dentate $SST^+$ or $VIP^+$ interneurons had no effect on EdU incorporation and MCM2 expression by RGLs (Fig. 4e, f and Supplementary Fig. 6e). Thus, coupling of neuronal circuit activity to RGL behaviour seems to be distinctive of $PV^+$ interneurons rather than occurring broadly across different local interneuron subtypes.

Finally, we assessed whether GABA also serves as a niche signal to mediate experience-dependent regulation of RGLs. We subjected mice to a social isolation regime, which decreases neuronal activity in the adult dentate gyrus[18] and was recently shown to promote RGL expansion[8]. Clonal analysis at 7 days after induction showed that, in contrast with group housing, social isolation led to a significant increase in $GFP^+$ RGL activation and symmetrical and astrogenic division, in a similar manner to $\gamma_2$ deletion in RGLs (Fig. 5a, b and Supplementary Fig. 7a). $\gamma_2$-deficient RGLs showed no additional activation or fate alternation after social isolation (Fig. 5b). At the population level, EdU incorporation and MCM2 expression by RGLs were increased significantly after social isolation (Fig. 5c and Supplementary Fig. 7b, c). $PV^+$ interneuron activation abolished the increase in RGL activation induced by social isolation (Fig. 5c). Thus, dentate $PV^+$ interneurons also mediate experience-dependent regulation of adult qNSCs through GABA-$\gamma_2$ signalling.

Precise control of somatic stem cell activity is essential for the long-term maintenance of tissue homeostasis and needs to be closely linked to tissue demands at any given time. Our study of adult RGLs at both clonal and population levels identified a previously unknown niche mechanism that regulates both adult qNSC activation and self-renewal mode in response to neuronal activity and experience (Supplementary Fig. 8). GABA has been shown to decrease the proliferation of other stem cells and progenitors *in vitro*, including mouse embryonic stem

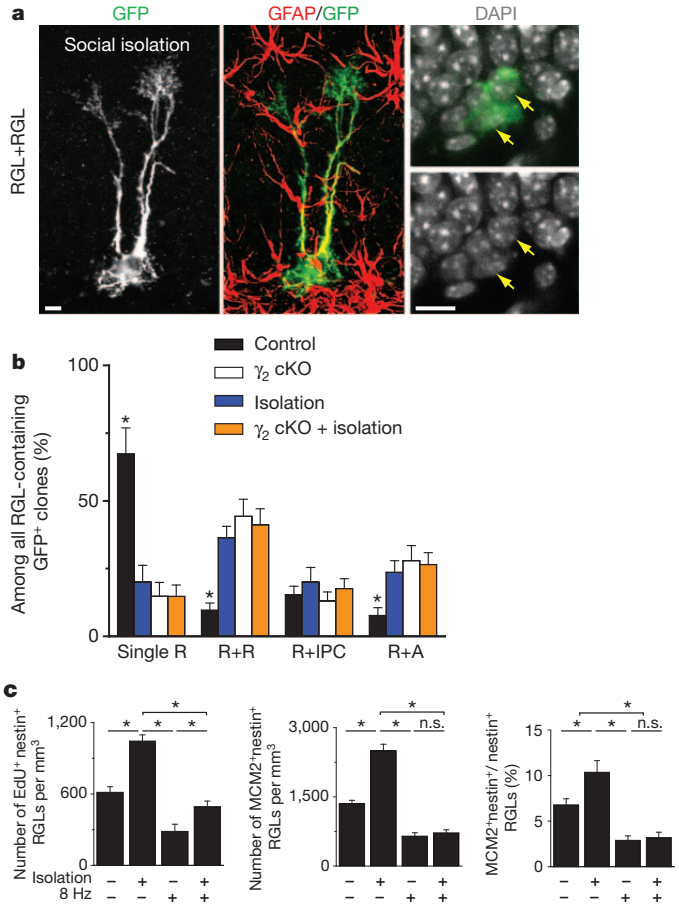


**Figure 5 | Contribution of GABA signalling from PV$^+$ interneurons to experience-dependent regulation of adult quiescent neural stem cells.** **a**, **b**, Clonal analysis of RGL fate choice after social isolation. **a**, Sample confocal images of immunostaining for an activated clone with two RGLs at 7 days after induction after social isolation (see Supplementary Fig. 7 for experimental procedure). Scale bars, 10 μm. **b**, Summary of different types of clone at 7 days after induction. Values are means and s.e.m. ($n = 4$–8 animals; asterisk, $P < 0.05$; Student's $t$-test). **c**, Summaries of stereological quantification of RGL EdU incorporation and MCM2 expression. Values are means and s.e.m. ($n = 4$ animals; asterisk, $P < 0.05$; n.s., $P > 0.1$; Student's $t$-test).

cells, by means of $GABA_A$Rs, the phosphatidylinositol-3-OH kinase (PI(3)K)-related kinase family and the histone variant H2AX[19,20]. PTEN deletion in individual RGLs also leads to activation and symmetrical self-renewal in the adult dentate gyrus[9], suggesting a conserved mechanism regulating the proliferation of various stem cells through the $GABA_A$R and PI(3)K/PTEN pathway.

Our optogenetic approach identified PV$^+$ interneurons as a critical and unique niche component among different interneuron subtypes that couples neuronal circuit activity to qNSC regulation *in vivo* under both physiological conditions and in response to specific experience. PV$^+$ interneurons are abundant in the hippocampus and have been implicated in higher brain function and cognitive dysfunction[15]. In the adult dentate gyrus, PV$^+$ interneurons receive excitatory inputs from dentate granule cells and, to a smaller extent, from entorhinal cortical inputs (Supplementary Fig. 8a). We reconstructed one PV$^+$ interneuron in the adult *PV-Cre*$^{+/-}$;*nestin–GFP*$^{+/-}$ mice and estimated that it covered more than 200 GFP$^+$ RGLs in the dentate gyrus (Supplementary Movie 3). A characteristic feature of PV$^+$ interneurons is the formation of ensembles coupled by both electrical (through gap junctions) and chemical connections (through reciprocal innervations)[15]. Thus, PV$^+$ interneurons are well suited to couple local circuit activity to the regulation of a large number of adult NSCs in the hippocampus as an adaptive mechanism—increasing qNSC activation when local circuitry activity levels are low, while keeping NSCs in quiescence when activity levels are high (Supplementary Fig. 8b). Given that both the number and properties of hippocampal PV$^+$ interneurons are regulated by physiological and pathological conditions, such as ageing, Alzheimer's diseases, epilepsy, chronic stress, schizophrenia and other severe psychiatric illness[21–26], our findings have broad implications.

## METHODS SUMMARY

Wild-type (C57BL/6), *nestin–GFP*[10], *PV-Cre*[17], *SST-Cre*[16], *VIP-Cre*[16], *nestin-CreER*$^{T2+/-}$;*Z/EG*$^{f/-}$;$\gamma_2^{f/f}$ (ref. 27) were used in the present study. Cre-dependent recombinant AAV[17] was used for interneuron subtype-specific expression of opsins in the adult dentate gyrus. Electrophysiological recordings and analysis were performed as described previously[28]. Immunohistochemistry, confocal imaging and processing were performed as described previously[9]. Stereological quantification was assessed as described previously[29]. All analyses were performed by investigators blind to experimental conditions. All animal procedures were performed in accordance with institutional guidelines.

**Full Methods** and any associated references are available in the online version of the paper at www.nature.com/nature.

**Received 10 November 2011; accepted 11 June 2012.**
**Published online 29 July 2012.**

1. Zhao, C., Deng, W. & Gage, F. H. Mechanisms and functional implications of adult neurogenesis. *Cell* **132,** 645–660 (2008).
2. Kriegstein, A. & Alvarez-Buylla, A. The glial nature of embryonic and adult neural stem cells. *Annu. Rev. Neurosci.* **32,** 149–184 (2009).
3. Ming, G. L. & Song, H. Adult neurogenesis in the mammalian brain: significant answers and significant questions. *Neuron* **70,** 687–702 (2011).
4. Seri, B., Garcia-Verdugo, J. M., McEwen, B. S. & Alvarez-Buylla, A. Astrocytes give rise to new neurons in the adult mammalian hippocampus. *J. Neurosci.* **21,** 7153–7160 (2001).
5. Lagace, D. C. *et al.* Dynamic contribution of nestin-expressing stem cells to adult neurogenesis. *J. Neurosci.* **27,** 12623–12629 (2007).
6. Imayoshi, I. *et al.* Roles of continuous neurogenesis in the structural and functional integrity of the adult forebrain. *Nature Neurosci.* **11,** 1153–1161 (2008).
7. Encinas, J. M. *et al.* Division-coupled astrocytic differentiation and age-related depletion of neural stem cells in the adult hippocampus. *Cell Stem Cell* **8,** 566–579 (2011).
8. Dranovsky, A. *et al.* Experience dictates stem cell fate in the adult hippocampus. *Neuron* **70,** 908–923 (2011).
9. Bonaguidi, M. A. *et al.* *In vivo* clonal analysis reveals self-renewing and multipotent adult neural stem cell characteristics. *Cell* **145,** 1142–1155 (2011).
10. Encinas, J. M., Vaahtokari, A. & Enikolopov, G. Fluoxetine targets early progenitor cells in the adult brain. *Proc. Natl Acad. Sci. USA* **103,** 8233–8238 (2006).
11. Farrant, M. & Nusser, Z. Variations on an inhibitory theme: phasic and tonic activation of $GABA_A$ receptors. *Nature Rev. Neurosci.* **6,** 215–229 (2005).
12. Bekkers, J. M. & Stevens, C. F. NMDA and non-NMDA receptors are co-localized at individual excitatory synapses in cultured rat hippocampus. *Nature* **341,** 230–233 (1989).
13. Caraiscos, V. B. *et al.* Tonic inhibition in mouse hippocampal CA1 pyramidal neurons is mediated by $\alpha_5$ subunit-containing γ-aminobutyric acid type A receptors. *Proc. Natl Acad. Sci. USA* **101,** 3662–3667 (2004).
14. Jagasia, R. *et al.* GABA-cAMP response element-binding protein signaling regulates maturation and survival of newly generated neurons in the adult hippocampus. *J. Neurosci.* **29,** 7966–7977 (2009).
15. Freund, T. F. & Buzsaki, G. Interneurons of the hippocampus. *Hippocampus* **6,** 347–470 (1996).
16. Taniguchi, H. *et al.* A resource of Cre driver lines for genetic targeting of GABAergic neurons in cerebral cortex. *Neuron* **71,** 995–1013 (2011).
17. Cardin, J. A. *et al.* Driving fast-spiking cells induces gamma rhythm and controls sensory responses. *Nature* **459,** 663–667 (2009).
18. Ibi, D. *et al.* Social isolation rearing-induced impairment of the hippocampal neurogenesis is associated with deficits in spatial memory and emotion-related behaviors in juvenile mice. *J. Neurochem.* **105,** 921–932 (2008).
19. Andang, M. *et al.* Histone H2AX-dependent $GABA_A$ receptor regulation of stem cell proliferation. *Nature* **451,** 460–464 (2008).
20. Fernando, R. N. *et al.* Cell cycle restriction by histone H2AX limits proliferation of adult neural stem cells. *Proc. Natl Acad. Sci. USA* **108,** 5837–5842 (2011).
21. Lolova, I. & Davidoff, M. Age-related morphological and morphometrical changes in parvalbumin- and calbindin-immunoreactive neurons in the rat hippocampal formation. *Mech. Ageing Dev.* **66,** 195–211 (1992).
22. Satoh, J., Tabira, T., Sano, M., Nakayama, H. & Tateishi, J. Parvalbumin-immunoreactive neurons in the human central nervous system are decreased in Alzheimer's disease. *Acta Neuropathol.* **81,** 388–395 (1991).
23. Masiulis, I., Yun, S. & Eisch, A. J. The interesting interplay between interneurons and adult hippocampal neurogenesis. *Mol. Neurobiol.* **44,** 287–302 (2011).
24. Knable, M. B., Barci, B. M., Webster, M. J., Meador-Woodruff, J. & Torrey, E. F. Molecular abnormalities of the hippocampus in severe psychiatric illness:

postmortem findings from the Stanley Neuropathology Consortium. *Mol. Psychiatry* **9,** 609–620 (2004).
25. Gonzalez-Burgos, G., Fish, K. N. & Lewis, D. A. GABA neuron alterations, cortical circuit dysfunction and cognitive deficits in schizophrenia. *Neural Plast.* **2011,** 723184 (2011).
26. Andre, V., Marescaux, C., Nehlig, A. & Fritschy, J. M. Alterations of hippocampal GABAergic system contribute to development of spontaneous recurrent seizures in the rat lithium-pilocarpine model of temporal lobe epilepsy. *Hippocampus* **11,** 452–468 (2001).
27. Schweizer, C. *et al.* The $\gamma_2$ subunit of $GABA_A$ receptors is required for maintenance of receptors at mature synapses. *Mol. Cell. Neurosci.* **24,** 442–450 (2003).
28. Ge, S. *et al.* GABA regulates synaptic integration of newly generated neurons in the adult brain. *Nature* **439,** 589–593 (2006).
29. Kim, J. Y. *et al.* DISC1 regulates new neuron development in the adult brain via modulation of AKT-mTOR signaling through KIAA1212. *Neuron* **63,** 761–773 (2009).

**Supplementary Information** is linked to the online version of the paper at www.nature.com/nature.

**Acknowledgements** We thank L. H. Tsai for initial help in the study; members of the Song and Ming laboratories for discussion; H. Davoudi for help; and Q. Hussaini, Y. Cai and L. Liu for technical support. This work was supported by grants from the National Institutes of Health (NIH) (NS047344) to H.S., the NIH (NS048271, HD069184), the National Alliance for Research on Schizophrenia and Depression and the Adelson Medical Research Foundation to G.L.M., the NIH (MH089111) to B.L., the NIH (AG040209) and New York State Stem Cell Science and the Ellison Medical Foundation to G.E., and by postdoctoral fellowships from the Life Sciences Research Foundation to J.S. and from the Maryland Stem Cell Research Fund to J.S., C.Z. and K.C.

**Author Contributions** J.S. led the project and contributed to all aspects. C.Z., M.A.B., G.J.S., D.H. and K.C. helped with some experiments. Y.G. and S.G. contributed reagents. J.H. provided *SST-Cre* mice. G.E. provided *nestin–GFP* mice. K.D. and K.M. provided initial help on optogenetic tools. B.L. provided $\gamma_2^{f/f}$ mice. J.S., G-l.M. and H.S. designed experiments and wrote the paper.

**Author Information** Reprints and permissions information is available at www.nature.com/reprints. The authors declare no competing financial interests. Readers are welcome to comment on the online version of this article at www.nature.com/nature. Correspondence and requests for materials should be addressed to H.S. (shongju1@jhmi.edu) or G.M. (gming1@jhmi.edu).

## METHODS

**Animals, housing, administration of tamoxifen, EdU and AAV, and optogenetic manipulations.** The following genetically modified mice and crosses between them were used for electrophysiological analysis: *nestin–GFP*[10] (CB57BL/6 background), *PV-Cre*[17] (JAX laboratory; stock number 008069; stock name B6;129P2-*Pvalb*$^{tm1(cre)Arbr}$/J), *SST-Cre*[16] (JAX laboratory; stock number 013044; stock name *Sst*$^{tm2.1(cre)Zjh}$/J), *VIP-Cre*[16] (JAX laboratory, stock number 010908; stock name *Vip*$^{tm1(cre)Zjh}$/J). The following mice were used for neurogenesis analysis: wild-type (C57BL/6), *nestin-CreER*$^{T2+/-}$;*Z/EG*$^{+/-}$;$\gamma_2^{floxed/floxed}$ (ref. 27; C57BL/6) and *nestin-CreER*$^{T2+/-}$;*Z/EG*$^{+/-}$ (C57BL/6), *PV-Cre* (B6;129), *SST-Cre* (B6;129), and *VIP-Cre* (B6;129). Animals were housed in a standard 14 h light/10 h dark cycle. Socially isolated animals were individually housed immediately after weaning for at least 6 weeks before injection with tamoxifen or EdU, and had free access to food and water[8]. A single dose of tamoxifen (62 mg kg$^{-1}$) was injected intraperitoneally into 6–10-week-old mice as described previously[9].

For optogenetic manipulations, Cre-dependent recombinant AAV vectors were used based on a DNA cassette carrying two pairs of incompatible loxP sites with the opsin genes (ChR2-H134–mCherry, ChR2-H134–YFP or eNpHR3.0–YFP) inserted between lox sites in the reverse orientation as described previously[17] (Supplementary Fig. 4a). The recombinant AAV vectors were serotyped with AAV2/9 for ChR2 (packaged at the UPenn Vector Core) and with AAV9 for eNpHR3.0 (packaged at University of North Carolina Vector Core). The following final viral concentrations were used for AAV viruses ($\times 10^{12}$ particles ml$^{-1}$): 7.4 (ChR2–YFP), 36 (ChR2–mCherry) and 8 (eNpHR3.0–YFP), respectively. AAV was delivered stereotactically into the dentate gyrus with the following coordinates (in mm): anterioposterior = −2 from bregma; lateral = ±1.5; ventral = 2.2. Fibre optic cannulae (Doric Lenses, Inc.) were implanted at the same injection sites immediately after AAV injection with a dorsal–ventral depth of 1.6 mm from the skull. Animals were then allowed to recover for at least 4 weeks after surgery. For analysis of RGL activation at the population level after optogenetic manipulations, littermates of animals were used and an *in vivo* light regime was administered 8 h per day for five consecutive days (Supplementary Figs 5a, 6e and 7b). For ChR2–YFP stimulation, flashes of blue light (472 nm; 5 ms at 8 Hz) through the DPSSL laser system (Laser Century Co. Ltd) were delivered *in vivo* every 5 min for 30 s per trial. For eNpHR–YFP stimulation, continuous yellow light (593 nm) was delivered *in vivo*. On the fifth day, animals were injected with EdU (41.1 mg per kg body weight) six times with an interval of 2 h. Animals were killed 2 h after the last EdU injection and were processed for immunostaining as described previously[9].

All animal procedures were performed in accordance with institutional guidelines.

**Electrophysiology.** Mice were anaesthetized and processed for slice preparation as described previously[28]. In brief, brains were quickly removed into the ice-cold solution (in mM: 110 choline chloride, 2.5 KCl, 1.3 $KH_2PO_4$, 25.0 $NaHCO_3$, 0.5 $CaCl_2$, 7 $MgSO_4$, 20 dextrose, 1.3 sodium L-ascorbate, 0.6 sodium pyruvate, 5.0 kynurenic acid). Slices 300 μm thick were sectioned with a vibratome (Leica VT1000S) and transferred to a chamber containing the external solution (in mM: 125.0 NaCl, 2.5 KCl, 1.3 $KH_2PO_4$, 1.3 $MgSO_4$, 25.0 $NaHCO_3$, 2 $CaCl_2$, 1.3 sodium L-ascorbate, 0.6 sodium pyruvate, 10 dextrose, pH 7.4, 320 mOsM), bubbled with 95% $O_2$/5% $CO_2$. Electrophysiological recordings were obtained at 32–34 °C. GFP$^+$ RGLs located within the SGZ in adult *nestin–GFP*$^{+/-}$ mice were revealed by differential interference contrast and fluorescence microscopy. A whole-cell patch-clamp configuration was employed in the voltage-clamp mode ($V_m$ = −65 mV) or current-clamp mode. Microelectrodes (4–6 MΩ) were pulled from borosilicate glass capillaries and filled with the internal solution containing (in mM)[28] 135 CsCl gluconate, 15 KCl, 4 $MgCl_2$, 0.1 EGTA, 10.0 HEPES, 4 ATP (magnesium salt), 0.3 GTP (sodium salt) and 7 phosphocreatine (pH 7.4, 300 mOsM). All RGL recordings were performed in the presence of kynurenic acid (5 mM). Data were collected with an Axon 200B amplifier and acquired with a DigiData 1322A (Axon Instruments) at 10 kHz. For measuring GABA-induced responses from GFP$^+$ RGLs, focal pressure ejection of 200 mM GABA or muscimol through a puffer pipette controlled by a Picospritze (2 s puff at 3–5 lb in$^{-2}$) was used to activate $GABA_A$Rs under the whole-cell voltage-clamp. A bipolar electrode (World Precision Instruments) was used to stimulate (0.1 ms duration) the dentate granule cell layer. Low-frequency stimuli (0.1 Hz) and theta bursts (8 Hz with a train of 100 stimuli) were delivered. The stimulus intensity (50 μA) was maintained for all experiments. The following pharmacological agents were used: diazepam (1 μM), NO-711 (10 μM), flumazenil (10 μM), midazolam (10 μM), ETMD (10 μM), L-655708 (50 μM) and vigabatrin (100 μM). All drugs were purchased from Sigma except bicuculline (50 or 100 μM; Tocris).

RGL recordings under optogenetic manipulation in acute brain slices were performed at least 4 weeks after injection with AAV. To stimulate ChR2 in labelled interneurons, light flashes (5 ms at 1, 8 or 100 Hz) generated by a Lambda DG-4 plus high-speed optical switch with a 300 W Xenon lamp and a 472 nm filter set (Chroma) were delivered to coronal sections through a ×40 objective lens (Carl Zeiss). To stimulate eNpHR in labelled interneurons, continuous yellow light generated by a DG-4 plus system with a 593 nm filter set were delivered to coronal sections across a full high-power (×40) field.

**Immunohistochemistry, confocal imaging, processing and quantification.** For immunostaining with anti-nestin and anti-MCM2, an antigen retrieval protocol was performed by microwaving sections in boiled citric buffer for 7 min as described previously[9]. For $\gamma_2$ immunostaining, a weak fixation protocol using live tissues was adopted as described previously[29,30]. For characterization of different interneuron subtypes, the following antibodies were used: anti-PV (Swant; mouse or rabbit; 1:500 dilution), anti-GAD-67 (Millipore; mouse or rabbit; 1:500 dilution), anti-SST (Millipore; rat; 1:200 dilution) and anti-VIP (Immunostar; rabbit; 1:200 dilution). For clonal analysis, coronal brain sections (40 μm) through the entire dentate gyrus were collected in a serial order, and immunostaining was performed with the following primary antibodies as described previously[9]: anti-GFP (Rockland; goat; 1:500 dilution), anti-nestin (Aves; chick; 1:500 dilution), anti-MCM2 (BD; mouse; 1:500 dilution), anti-GFAP (Millipore; mouse or rabbit; 1:1,000 dilution) and anti-PSA-NCAM (Millipore, mouse lgM; 1:500 dilution). For quantification of GFP$^+$ clones at 2 and 7 days after induction, a single GFP$^+$ RGL was scored as a quiescent clone. Two or more nuclei in a GFP$^+$ RGL clone were scored as activation. Clonal analysis at 30 days after induction was conducted exactly as described previously[9].

For experiments with diazepam (5 mg kg$^{-1}$ body weight; once daily for 5 days), coronal brain sections (40 μm) through the entire dentate gyrus were collected in a serial order. For optogenetic manipulations, sections within a distance of 1.0 mm anterior and 1.0 mm posterior to injection sites were used for quantification, given the estimated light spread *in vivo*. Immunostaining was performed on every sixth section as described previously[9]. EdU labelling was performed with a Click-iT EdU Alexa Fluor imaging kit (Invitrogen). Images were acquired on a Zeiss LSM 710 confocal system (Carl Zeiss) with a ×40 objective lens using a multitrack configuration. Stereological quantification of cells positive for various molecular markers was assessed in the dentate gyrus with a modified optical fractionator technique[29]. For quantification of EdU$^+$ or MCM2$^+$ RGLs, an inverted 'Y' shape from anti-nestin staining superimposed on EdU$^+$ or MCM2$^+$ nucleus was scored double positive for nestin and EdU or MCM2. All analyses were performed by investigators blind to experimental conditions. Statistical analysis was performed with Student's *t*-test.

For generation of movie files, images were serially reconstructed in Reconstruct (J. C. Fiala, NIH), normalized, and deconvolved with Autoquant X2 (Media Cybernetics). Images were then segmented in MATLAB (The Mathworks) using custom code and imported into Imaris (Bitplane). Surface renderings and movies were made using the Surface and Animation functions, respectively, in Imaris (Supplementary Movies 1–3).

30. Schneider Gasser, E. M. *et al.* Immunofluorescence in brain sections: simultaneous detection of presynaptic and postsynaptic proteins in identified neurons. *Nature Protocols* **1,** 1887–1897 (2006).